


EXPRESS LETTER

Open Access



Aeromagnetic survey in Kusatsu-Shirane volcano, central Japan, by using an unmanned helicopter

Takao Koyama^{1*} , Wataru Kanda², Mitsuru Utsugi³, Takayuki Kaneko¹, Takao Ohminato¹, Atsushi Watanabe¹, Hiroshi Tsuji¹, Taro Nishimoto¹, Alexey Kuvshinov^{1,4} and Yoshiaki Honda⁵

Abstract

Kusatsu-Shirane volcano is one of the active volcanoes in Japan. Phreatic explosions occurred in Mt. Shirane in 1983 and most recently, in 2018, in Mt. Motoshirane. Information on the subsurface structure is crucial for understanding the activity of volcanoes with well-developed hydrothermal systems where phreatic eruptions occur. Here, we report aeromagnetic surveys conducted at low altitudes using an unmanned helicopter. The survey aimed to obtain magnetic data at a high spatial resolution to map the magnetic anomaly and infer the magnetization intensity distribution in the region immediately after the 2018 Mt. Motoshirane eruption. The helicopter used in the survey was YAMAHA FAZER R G2, an autonomously driven model which can fly along a precisely programmed course. The flight height above the ground and a measurement line spacing were set to ~ 150 m and ~ 100 m, respectively, and the total flight distance was 191 km. The measured geomagnetic total intensity was found to vary by ~ 1000 nT peak-to-peak. The estimated magnetization intensity derived from measured data showed a 100 m thick magnetized surface layer with normal polarity, composed of volcanic deposits of recent activities. Underneath, a reverse-polarity magnetization was found, probably corresponding to the Takai lava flow in the Early Quaternary period (~ 1 Ma) mapped in the region. Our results demonstrate the cost-effectiveness and accuracy of using drone magnetometers for mapping the rugged terrain of volcanoes.

Keywords: Kusatsu-Shirane volcano, Aeromagnetic survey, Unmanned helicopter

Introduction

Kusatsu-Shirane volcano is one of the most active volcanoes located in the central part of Japan. In the area surrounding Kusatsu-Shirane volcano, some Quaternary volcanoes have formed over the Early Quaternary or Tertiary andesitic basement rocks (e.g., Hayakawa and Yui 1989; Terada 2018). At the first stage of the formation history of Kusatsu-Shirane volcano, Matsuozawa lava flow erupted at ~0.5 Ma, followed by the Horaguchi lava and Oshi pyroclastic flows (Kaneko et al. 1991).

Following another eruptive stage, the three main pyroclastic cones, Mt. Shirane, Mt. Ainomine, and Mt. Motoshirane, formed approximately 10,000 years ago and are covered by volcanic deposits with a thickness of a few 100 m (Hayakawa and Yui 1989). Recent activities were almost only observed in Mt. Shirane, and frequent phreatic explosions occurred every couple of 10 years.

Mt. Ainomine and Mt. Motoshirane have been inactive for 1500 years (Nigorikawa et al. 2016). At the east flank of Mt. Motoshirane, however, there is a large amount of strong acidic hot spring water discharged (as much as 10 ton per minute; Kikawada et al. 2008), implying that a notable widespread hydrothermal system exists beneath Kusatsu-Shirane volcano (e.g., Ohba et al. 2000).

*Correspondence: tkoyama@eri.u-tokyo.ac.jp

¹ Earthquake Research Institute, The University of Tokyo, Yayoi 1-1-1, Bunkyo-ku, Tokyo 113-0032, Japan

Full list of author information is available at the end of the article

In active volcanoes with an aquifer, phreatic explosions occur because of the interaction of hot volcanic volatiles with groundwater. Mt. Shirane has experienced such eruptions. Phreatic explosions are usually not preceded by apparent precursory events; thus, it is difficult to predict their occurrence, which consequently leads to damages and casualties. The detection of tiny geophysical and geochemical signals preceding phreatic explosions as well as geological knowledge of the volcano is the key to accurate and timely predictions (Terada 2018).

The current grounded survey was carried out mainly at Mt. Shirane as it was recently active. Takahashi and Fujii (2014) revealed, through repeated ground-based geomagnetic surveys, the long-term thermomagnetic variations corresponding to volcanic activities caused by magnetizing or demagnetizing sources beneath the crater of Mt. Shirane. Tokyo Institute of Technology installed permanent stations of the magnetometer. In 2014, microseismic swarms and geomagnetic changes were detected at the same time in Mt. Shirane. The stations nearest to the Yugama crater showed a rapid decrease in geomagnetic total intensity. This implies that thermal demagnetization occurred just east of the Yugama crater of Mt. Shirane (Hashimoto et al. 2019). These geomagnetic changes may indicate that volcanic activity is getting gradually activated. In contrast, due to a lack of activity, Mt. Motoshirane was considered less likely to erupt than Mt. Shirane and hence, neither geomagnetic nor seismic stations were deployed in the region.

On January 23, 2018, however, there was a phreatic explosion at the Kagamiike-kita pyroclastic cone of Mt. Motoshirane (Ogawa et al. 2018). Volcanic activity on Mt. Motoshirane was low until then and the eruption was unexpected. The estimated mass of volcanic products in this event was not much, being less than 40 thousand tons (Ogawa et al. 2018; Himematsu et al. 2020), but some casualties happened because of lack of preparedness.

Matsunaga et al. (2020) revealed the electrical conductivity structure of Mt. Motoshirane by magnetotelluric surveys. They detected a surface clay-rich alteration layer, ~0.5 km thick, and a deep and wide conductor which is interpreted to be a hydrothermal fluid reservoir. This reservoir can be a root of volcanic earthquakes occurring beneath Mt. Motoshirane and can also provide volcanic fluid mixed with meteoric water to the hot springs on the eastern flank of Mt. Motoshirane. A resistive body was also detected, which corresponds with basement rocks due to the geological results (Hayakawa and Yui 1989). Tseng et al. (2020) also revealed the electrical conductivity beneath the crater lake, Yugama, of Mt. Shirane, and detected a pathway between Yugama and a deep reservoir. These previous results imply that Kusatsu-Shirane

volcano has a variable subsurface structure with some craters, and it is very important to understand it.

We conducted aeromagnetic surveys, with high spatial resolution, to elucidate the Kusatsu-Shirane volcano. Aeromagnetic surveys are used to investigate the inside of the volcanoes to detect thermal anomalies due to demagnetization of subsurface rocks and predict potential eruptive events (e.g., Nakatsuka 1994; Okuma et al. 1994; Finn et al. 2001; Okubo et al. 2005). We used an unmanned helicopter instead of a manually operated one to prevent safety hazards (Kaneko et al. 2011; Koyama et al. 2013; Hashimoto et al. 2014; Ohminato et al. 2017).

In this paper, we have presented an aeromagnetic survey conducted using an unmanned helicopter and the data processing procedure, followed by the estimation of the magnetization intensity distribution to discuss the subsurface structure of Kusatsu-Shirane volcano.

Aeromagnetic survey in Kusatsu-Shirane volcano

We conducted aeromagnetic surveys of Kusatsu-Shirane volcano, central Japan, in 2018, immediately after the Mt. Motoshirane eruption in January 2018, by using an unmanned helicopter to acquire magnetic field data of high spatial resolution, mitigating potential safety concerns. The unmanned helicopter, YAMAHA FAZER R G2, is driven by an internal combustion engine, and can fly continuously for over 2 h. A common drawback of the usage of internal combustion engines is the lack of combustion efficiency due to decreasing oxygen concentration at high altitude, and the previous model, YAMAHA RMAX G1, did not have the capacity to fly beyond Kusatsu-Shirane volcano the altitude of which is 2171 m (Morimoto 2017). However, FAZER R G2 is a state-of-the-art vehicle with a four-stroke engine (Kido et al. 2016), and can be operated even at altitudes of 2800 m (Morimoto 2017). The helicopter provides advantages, such as safety, and also has the ability to fly along a preprogrammed course, owing to which it can fly along the same course repeatedly and can be very useful for repeated surveys to detect temporal changes in geomagnetic fields. The time and position of the helicopter were recorded accurately up to a few tens of centimeters in the horizontal direction and < 1 m in the vertical direction in a quiet wind condition.

A cesium optical pumping magnetometer (Geometrics G-858 MagMapper Magnetometer) was used to measure the scalar value of geomagnetic total intensity up to 0.1 nT accuracy (Geometrics 2001). Electric power to the magnetometer was supplied by the helicopter generator. Time calibration was performed by the 1 Hz time-stamping tool of a small portable GNSS device, Garmin eTrex H (Garmin 2007) via an RS-232C interface to the magnetometer. Note that positioning data acquired by

the portable device are generally not very accurate (more than a few meters accuracy) and the positioning data acquired by the helicopter were used instead in the data processing of this study. The time of measurement was adjusted after the survey flights, according to the time of the flight record, containing the precise position information. The console of the magnetometer was fixed to the helicopter body. A magnetic sensor was hung down with a 5.5 m sensor cable to be installed away from the helicopter body in order to reduce the effect of the vehicle magnetization field. Thus, the position of the magnetic sensor can be assumed to be 5.5 m beneath the recorded position of the helicopter. The expected total error of measurement is ~ 10 nT including the effects of a vehicle magnetization field and positioning error due to the swinging of the sensor.

The total weight of magnetometer was ~ 4 kg, which was much less than the maximum payload of the helicopter (35 kg; Morimoto 2017). Measurements were taken at 10 Hz sampling. The flight speed was ~ 10 m/s, and the typical altitude above the ground was 150 m. A typical survey area measured ~ 3.5 km \times 3.5 km. The survey line spacing was ~ 100 m, and the total flight distance was ~ 191 km. Figure 1 shows a plane map of the flight courses, colored by the measurement value of geomagnetic total intensity. The measured geomagnetic total intensity anomaly was as high as 1000 nT. A reference station of geomagnetic total intensity was deployed 4 km away from the survey area to eliminate daily variation in geomagnetic total intensity due to the external geomagnetic field. The same model of the magnetometer Geometrics G-858 MagMapper Magnetometer was used. 10 Hz sampling was done during flights, which is the same rate as measured by a magnetometer on the helicopter, and 1 Hz sampling was done in the nighttime to determine a midnight mean value as a baseline.

Data processing and modeling

The observed geomagnetic total intensity data in the helicopter were decimated to 1 Hz sampling for precise position and time calibration by the GNSS receiver, and outliers, such as spike noises, were removed. Thereafter, the magnetic field of both the Earth's core and external origins were subtracted from these data to extract the geomagnetic field component only due to volcanic rock origin. The geomagnetic main field of the core origin was assumed to be expressed by the CHAOS-7 geomagnetic field model (Finlay et al. 2020). This main field model has a better time resolution than a common IGRF model published every 5 years, and it can provide the main field data more precisely. The time variation of the external origin was assumed to be identical to that at the reference station. The variation was estimated using the reference

field data by subtracting the midnight mean value. Finally, the extracted geomagnetic field data were decimated to provide evenly distributed spatial data, typically with 100 m spacing.

Using the calculated geomagnetic total intensity anomaly of volcanic origin, the magnetization intensity of Kusatsu-Shirane volcano was estimated, as the orientation of magnetization was assumed to be identical to the direction of the current geomagnetic main field in any position of our targeted area: inclination and declination are 51.0° downward and 7.9° westward, respectively.

The details of modeling are described in Appendix. Regarding the target volume V_{uni} , a much wider area than the survey area, 26 km \times 26 km, was considered to avoid artifacts of the edge effect of the model space. Surface topography was referred to as a digital elevation model with a 10 m horizontal square mesh published by GSI Japan. According to the locations of hypocenters, seismicity can be detected up to 1.5–2.0 km depth from the surface (e.g., Matsunaga et al. 2020), and brittle–ductile transition may occur at the bottom of the seismic region, at a depth of 1.4 km (Tseng et al. 2020). Thermal demagnetization of the andesitic rock of Mt. Shirane at 400°C may also occur at this depth (Yamazaki et al. 1992); thus, the magnetizing thickness was assumed to be 1500 m from the surface in this study. A target volume V_{uni} of 26 km \times 26 km \times 1.5 km was assumed to be magnetized, and other areas were assumed not to be magnetized at all. The uniform magnetization intensity m_{uni} was estimated as 0.97 A/m. This is close to the results of laboratory measurements of the andesitic rock sampled in Mt. Shirane (Yamazaki et al. 1992). Standard deviation of data misfit between observed data and synthetic data by this uniformly magnetized model was estimated as 134.4 nT, which is too large compared to the expected data error (~ 10 nT).

Regarding the three-dimensional inverse modeling, the target area was assumed to be 19 km \times 19 km, still much wider than the survey area, and the magnetizing thickness was again assumed to be 1500 m. A target volume, V_{ano} , of 19 km \times 19 km \times 1.5 km, was discretized by blocks with dimensions 250 m \times 250 m in horizontal spacing, and was divided vertically into four layers. The thicknesses of the four layers are 100, 200, 400, and 800 m from the top layer to the bottom, respectively. Each block was assumed to be uniformly magnetized. Note that each block is not an exact rectangular block, but has fluctuations at the top and bottom due to the topography with a horizontal resolution of 10 m.

Figure 2 shows data misfit between observed geomagnetic total intensity and synthetic data using an optimal model. Standard deviation of data misfit was estimated as 12.7 nT, which is close to an expected data error.

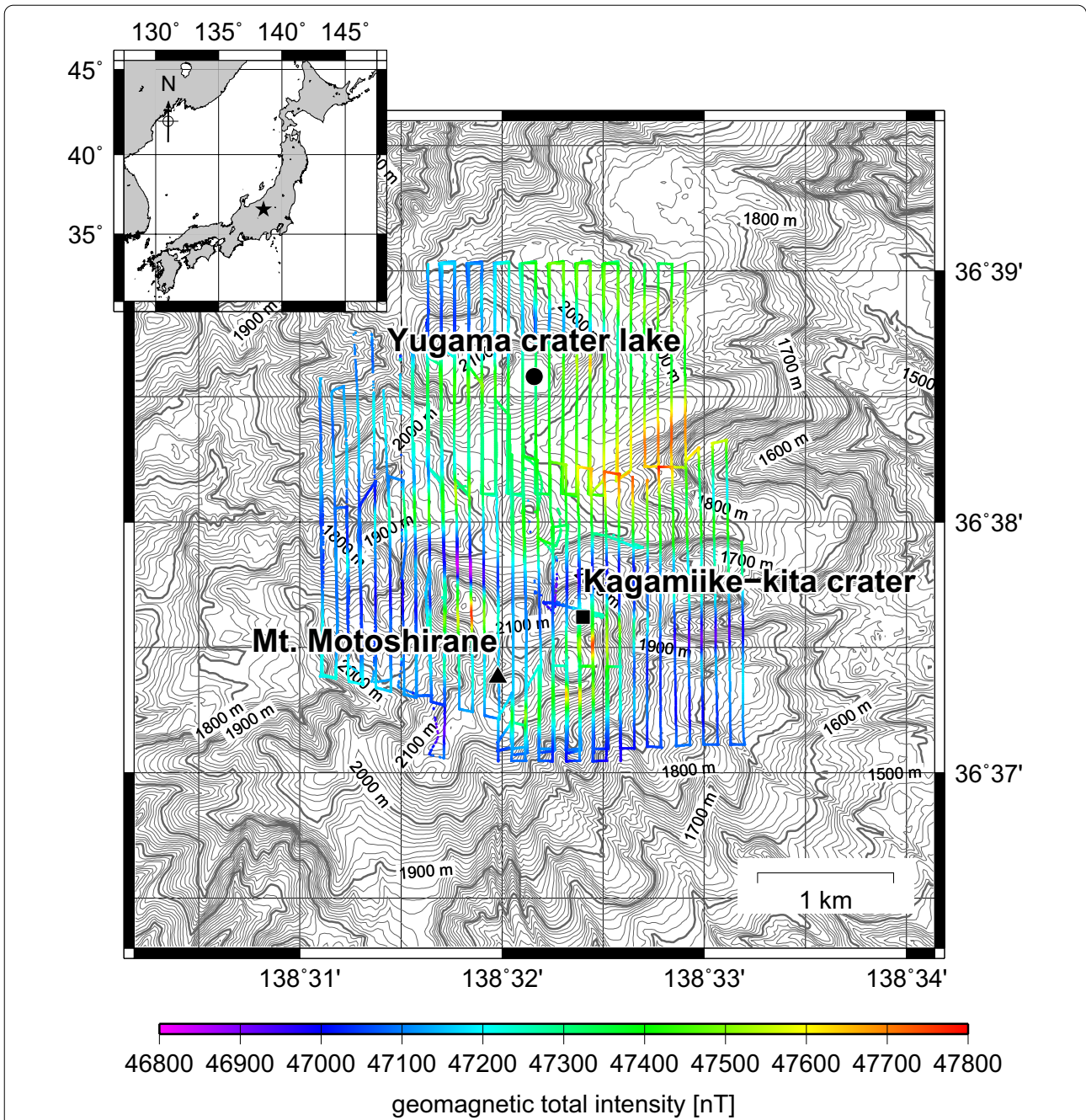


Fig. 1 Survey area map in Kusatsu-Shirane volcano: the flight course projected onto the plane map is color-contoured in the geomagnetic total intensity measured by the helicopter. The closed circle, square, and triangle indicate the locations of the crater lake Yugama of Mt. Shirane, Kagamiike-kita crater, and the main crater of Mt. Motoshirane, respectively. The star in the small map indicates the location of Kusatsu-Shirane volcano in Japan

Figure 3 shows the magnetization intensity distribution of each layer of the optimal model. Note that it shows only an area of our survey and surroundings, and does not show all the inverted model space. The model is well

inverted in the survey area over which the helicopter took flights. However, the model was not recovered in the area apart from the survey area due to the lack of sensitivity and model resolution.

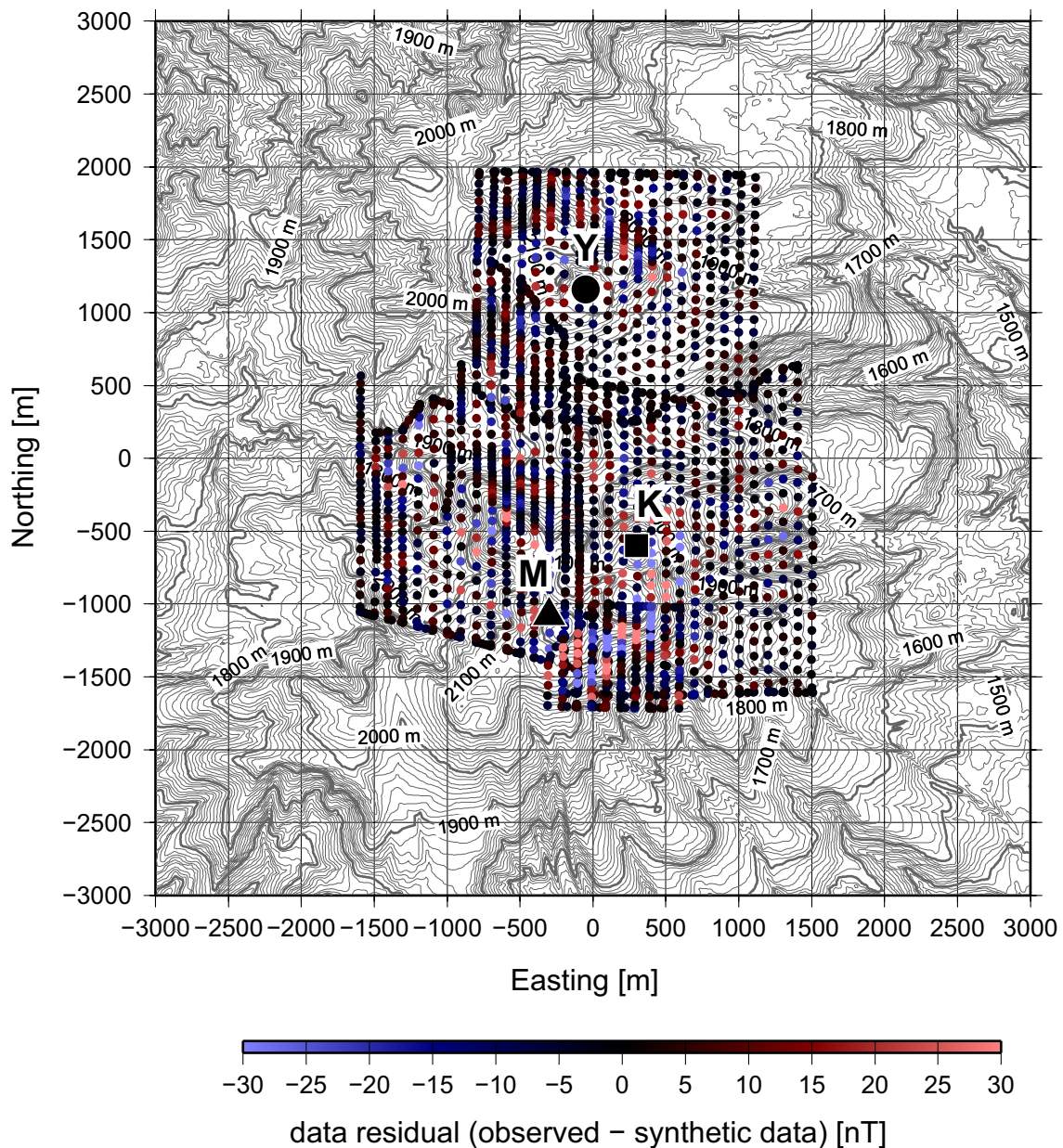


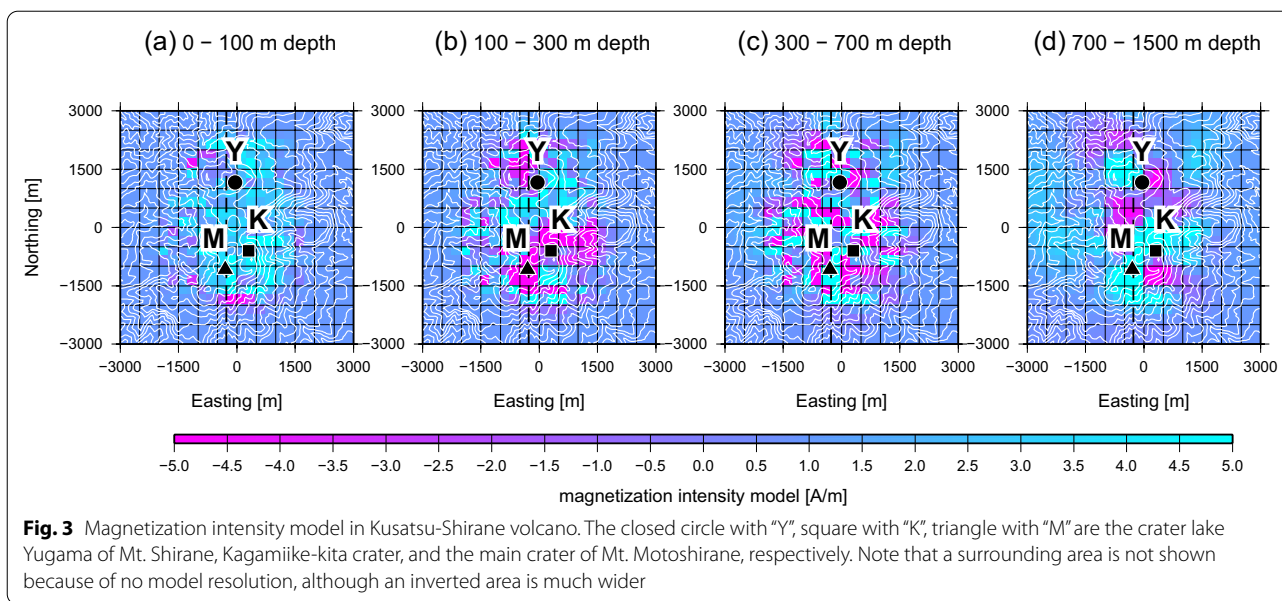
Fig. 2 Data residual between observed value and synthetic value by the optimal magnetization intensity model in Fig. 3. Standard deviation of data misfit is estimated as 12.7 nT. The closed circle with "Y", square with "K", triangle with "M" are the crater lake Yugama of Mt. Shirane, Kagamiike-kita crater, and the main crater of Mt. Motoshirne, respectively

Additional file 1: Figure S1 shows the deviation of model parameters, which is derived from the ABIC minimization shown in Appendix. The first layer is well resolved, and a deviation of model is less than 3.5 A/m; the second layer is deviated by 1.5–5.8 A/m. The third is deviated by 6 A/m or more. The fourth layer has no resolution, and the deviation is about 20 A/m. Thus,

hereafter, we discuss the magnetization in the first to the third layers.

Discussion

The top layer in Fig. 3a indicates that the entire surface is magnetized with positive polarity. A surface layer with a thickness of a few 100 m is composed of volcanic



deposits in the middle Quaternary activities (~0.5 Ma) of Kusatsu-Shirane volcano, such as Matsuzawa lava, Horaguchi lava, Oshi pyroclastic flow, and younger lava flows (Hayakawa and Yui 1989; Kaneko et al. 1991; Uto et al. 2004). Yamazaki et al. (1992) measured the remanent magnetization of pyroxene andesite, sampled close to Yugama Lake, and it exhibited the magnetization intensity as high as 1–2 A/m, which is consistent with a model in the top layer with weak anomalies.

The second and third layers, shown in Fig. 3b, c down to a depth of 700 m from the surface, however, indicate negative or almost zero magnetization over a wide area. Akimoto et al. (2002) found that an orientation of the rocks in Yatsugatake, 75 km south of Kusatsu-Shirane, in about 1 Ma is almost opposite to the orientation of a current main field. Thus, an area with negative magnetization can be interpreted as a reversely magnetized region. Although this might have been caused by overweighting on this layer in the inversion calculation, rocks at these depths may be constituted of basement rock in the early Quaternary, Takai lava. This lava is supposed to be approximately the same age as Omeshi volcano, west of Kusatsu-Shirane volcano (Kaneko et al. 1991). K–Ar dating by Kaneko et al. (1991) shows that the age of Omeshi volcano is 1.10 ± 0.09 Ma. This means that the Takai lava erupted in the early Quaternary which was in Matuyama reversed Chron. Nagai et al. (2015) investigated core data from a drill hole, 3 km west of Mt. Motoshirane, and found a tuff dating to 1.29 ± 0.06 Ma at 171.5 m depth or deeper. Hayakawa and Yui (1989) indicated that there is a long inactive stage, spanning a couple of hundred thousand

years between two eruptive stages, and the later eruptive stage may not have used magma, unerupted and solidified in the former eruptive stage. It may have cooled and magnetized lava stayed at this depth after the eruptive stage. Also, it might be highly altered and demagnetized, corresponding to a high conductive region of Takai lava (Matsunaga et al. 2020). Figure 4 shows the North–South vertical profile of the magnetization model through Yugama and Mt. Motoshirane, compared with the electrical resistivity model of Matsunaga et al. (2020). The second and third layers of magnetization model correspond to a conductive layer, which can be altered to clay. Therefore, it is consistent that the second and third layers appear less magnetized and partly reversely magnetized.

The detection of temporal changes in the geomagnetic total intensity by aeromagnetic measurements is very challenging. Figure 5 shows repeatability of data acquisition, that is, deviation of measured data for pairs of sites, which are closer than 5 (in gray color) and 10 (in white color) m to each other. A typical data error or standard deviation was as small as 10 nT or less in this survey. On the contrary, a temporal change detected by a ground-based survey was a few nT in the latest measurements (Hashimoto et al. 2019). It seems difficult to detect and is out of the scope of this research. Aeromagnetic survey, however, can measure a wide spatial pattern with high spatial resolution at precisely the same points, which means that spatial stacking to remove the noise can be performed. It may be possible to detect a minor geomagnetic change of volcanic origin with a wide spatial trend

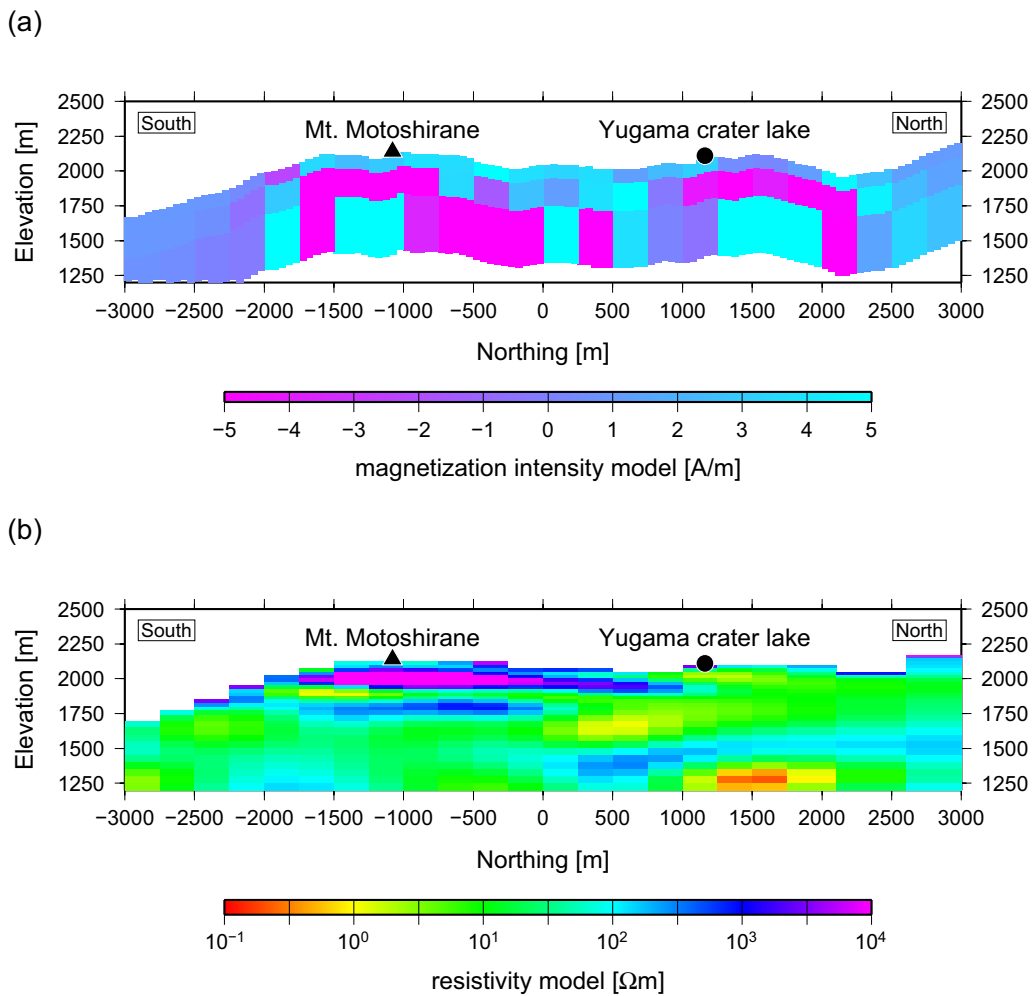


Fig. 4 **a** Vertical profile of the magnetization intensity model along a dashed line in Fig. 3, through Mt. Motoshirane (closed triangle) and Yugama crater lake of Mt. Shirane (closed circle). **b** Vertical profile of the electrical resistivity model by Matsunaga et al. (2020) on the same line of **a**

even within a noise of 10 nT by repeated airborne measurements in future surveys.

Conclusion

In this study, highly spatially resolved magnetic field data were acquired from Kusatsu-Shirane volcano, and a geomagnetic field anomaly of approximately 1000 nT was detected using an autonomously driven unmanned helicopter. A three-dimensional magnetization intensity distribution was elucidated by using the measured geomagnetic field data. It shows thin normally magnetized lava at the surface underlain by altered and reversely magnetized lavas. This implies that the main basement

lava, Takai lava, can be supposed to have erupted at the time in Matuyama reversed Chron, and have altered later.

Aeromagnetic surveys have shown the potential to elucidate the wide and deep distribution of magnetization. Recently, some studies have reported aeromagnetic surveys using a common drone, which can be easily performed at a low cost (e.g., Utsugi and Hashimoto 2016; Malehmir et al. 2017; Koyama et al. 2019). It can be significantly improved in the near future and can be utilized in volcanic surveys for the detection of temporal changes in the geomagnetic field due to volcanic activity by repeated surveys, combined with ground-based surveys.

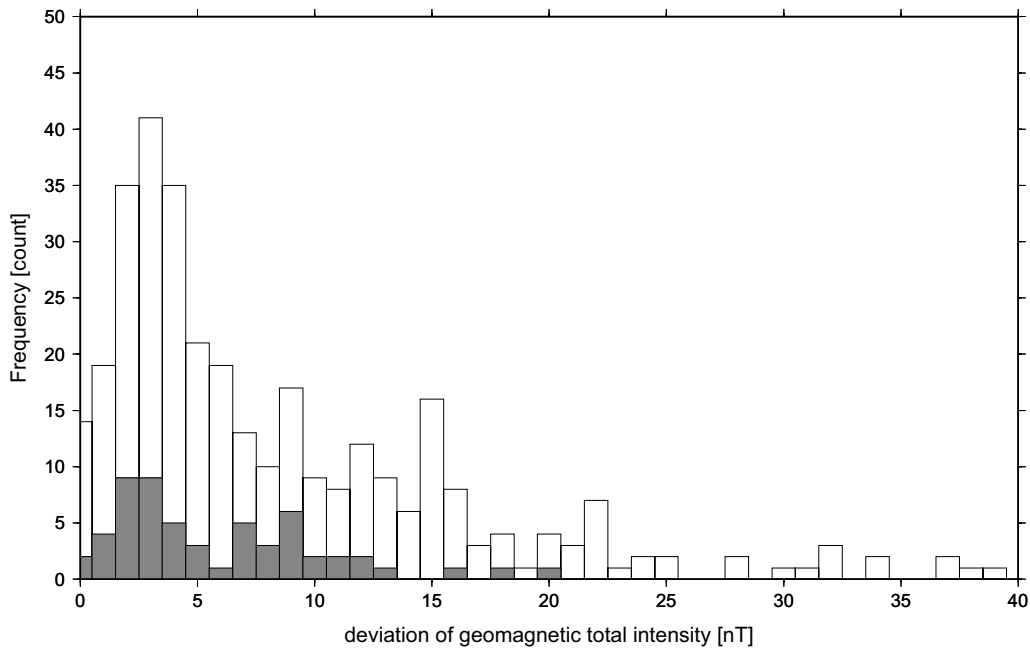


Fig. 5 Deviation of measured geomagnetic total intensity data between a pair of points closer than 5 (in gray color) and 10 (in white color) m of each other, which shows repeatability of data acquisition by unmanned helicopter

Appendix: Magnetization intensity inversion

In the first step, the average value of the magnetization intensity, that is, uniform magnetization intensity was estimated in the least squares sense for fitting all the data by removing the trend surface of the geomagnetic field anomaly, minimizing the following objective function, Φ_{uni} :

$$\Phi_{uni} = \sum_{n=1}^N \left\{ d_n(x_n, y_n, z_n) - m_{uni} \left(\iiint_{V_{uni}} K(x_n, y_n, z_n; x', y', z') dx' dy' dz' \right) - (a_0 + a_x x_n + a_y y_n + a_z z_n) \right\}^2, \quad (1)$$

where d_n is the n th data parameter, which is the measured geomagnetic total intensity subtracted by the core field by the CHAOS-7 model and the external field variation, (x_n, y_n, z_n) is a vector of the position of the geomagnetic sensor of the helicopter at the n th data parameter, and N is the total number of data parameters. The volume to be uniformly magnetized is given by V_{uni} , and $K(x_n, y_n, z_n; x', y', z')$ is a kernel that expressed the geomagnetic total intensity anomaly at position (x_n, y_n, z_n) generated by a unit magnetizing source at position (x', y', z') . The target uniform magnetization intensity is given by m_{uni} and $a_0 + a_x x + a_y y + a_z z$ is an assumed trend surface to be removed, where a_0, a_x, a_y and a_z are constant parameters and estimated as well as m_{uni} . The volume integral in Eq. (1) was derived by following a common formulation for a rectangular prism with magnetization (Bhattacharyya 1964; Kunaratnam 1981).

The next step is the estimation of three-dimensional anomaly of the magnetization intensity deviating from the average intensity. Various methods of three-dimensional inversion of magnetization have been proposed (e.g., Li and Oldenburg 1996; Nakatsuka and Okuma 2014; Utsugi 2019), and the two-dimensional inver-

sion method by Koyama et al. (2013) was adapted to the three-dimensional case in this study, which is a commonly used least squares method for fitting the data with model constraints for regularization to minimize the following objective function, Φ_{ano} .

$$\Phi_{ano} = \sum_{n=1}^N \{ d'_n(x_n, y_n, z_n) - \iiint_{V_{ano}} K(x_n, y_n, z_n; x', y', z') \Delta m(x', y', z') dV' \}^2 + \lambda \iiint_{V_{ano}} \{ w(x', y', z') \Delta m(x', y', z') \}^2 dV', \quad (2)$$

where d'_n is the geomagnetic total intensity anomaly of the n th data, subtracting components generated by a uniform structure and a trend surface. V_{ano} is the target volume for three-dimensional inversion. The magnetization intensity anomaly from a uniform model and the weight function on it are represented by $\Delta m(x', y', z')$ and $w(x', y', z')$, respectively.

The objective function, Φ_{ano} , in Eq. (2) can be rewritten using a discretized model anomaly parameter, Δm_m , as follows:

$$\Phi_{\text{ano}} = \sum_{n=1}^N \left\{ d'_n(x_n, y_n, z_n) - \sum_{m=1}^M KdV_m(x_n, y_n, z_n) \Delta m_m \right\}^2 + \lambda \sum_{m=1}^M \{w_m \Delta m_m\}^2, \tag{3}$$

where M is the total number of model parameters. $KdV_m(x_n, y_n, z_n)$ is a volume-integrated kernel for the m th model parameter, Δm_m . w_m is the weight of the m th model parameter. λ is a hyperparameter that balances the data misfit term and model constraint (or roughness) term, which are the first and second terms of the right-hand side of Eq. (3).

The model constraint or model roughness term is supposed to minimize the L2 norm of the weighted magnetization intensity anomaly model deviating from an average uniform magnetization intensity, m_{uni} . The weight of the model anomaly w_m is assumed to be the square root of the kernel of the model block to the position just above the block at a typical flight height above the ground.

$$w_m = \left| \int_{x_m - \frac{\Delta x}{2}}^{x_m + \frac{\Delta x}{2}} dx' \int_{y_m - \frac{\Delta y}{2}}^{y_m + \frac{\Delta y}{2}} dy' \int_{z_m(x', y')} dz' K(x_m, y_m, z_{\text{topo}} + \Delta z; x', y', z') \right|^{\frac{1}{2}}, \tag{4}$$

where (x_m, y_m) is the horizontal center position of the m th model block. Note that it is not identical to the weight function of Li and Oldenburg (2000), but our method avoids overweighting on blocks locating far from the survey area.

The hyperparameter, λ , to weigh the model constraint was determined by the ABIC minimization concept (e.g., Akaike 1980; Honsho et al. 2012; Koyama et al. 2013). An optimal hyperparameter could be uniquely determined to minimize the ABIC, and the ABIC minimization concept could select an optimal solution properly, even according to the L-curve criterion by Hansen (1992) (Additional file 2: Figure S2).

According to ABIC, a model covariance matrix C_M is derived as follows:

$$C_{M_{ij}} = \left[\frac{\left(\sum_{n=1}^N \{KdV_i(x_n, y_n, z_n) KdV_j(x_n, y_n, z_n)\} + \delta_{ij} \lambda w_i^2 \right)}{\Phi_{\text{ano}}/N} \right]^{-1},$$

where $C_{M_{ij}}$ is an element (i, j) of the matrix C_M . δ_{ij} is the Kronecker delta.

Thus, a square root of each diagonal element, $(C_{M_{mm}})^{1/2}$, can be supposed to simply represent a deviation of the m th model parameter, Δm_m .

Abbreviations

Ma: Million years ago; RS-232C: Recommended Standard 232 version C; GNSS: Global Navigation Satellite System; IGRF: The International Geomagnetic Reference Field; GSI Japan: The Geospatial Information Authority of Japan; ABIC: Akaike’s Bayesian information criterion.

Supplementary Information

The online version contains supplementary material available at <https://doi.org/10.1186/s40623-021-01466-5>.

Additional file 1: Figure S1. Deviation of model parameters of magnetization intensity model in Fig. 3, which is represented by a square root of each diagonal element of the estimated model covariance matrix by the ABIC minimization.

Additional file 2: Figure S2. (a) ABIC with a hyperparameter λ dependency. A closed circle is a minimum point of ABIC. (b) Data misfit and model roughness with a hyperparameter λ dependency. A closed circle corresponds to an optimal λ minimizing ABIC in (a).

Acknowledgements

A staff of the UMS Business Development Section, YAMAHA Motor Co., Ltd. operated the unmanned helicopter YAMAHA FAZER R G2 in entire surveys. Mr. Yasuo Matsunaga kindly shared the electrical conductivity model of Kusatsu-Shirane with us. The Editor and two anonymous reviewers gave useful comments to improve our manuscript. The Kusatsu town office, the Agatsuma District Forest Office, and the Manza Park Rangers Office granted approvals for the field surveys documented in this study. A digital elevation model with 10 m horizontal resolution was provided by GSI Japan. Figures in this paper were created partly using Generic Mapping Tools (Wessel et al. 2013).

Authors’ contributions

TKo and MU contributed to data acquisition and data analysis. WK contributed to planning, preparing and organizing of the survey as well as data acquisition. TKa, TO, AW, HT, TN, AK, and YH contributed to support data acquisition and safe flight of the unmanned helicopter. All authors read and approved the final manuscript.

Funding

This work was supported by JSPS KAKENHI Grant-in-Aid for Special Purposes Number 17K20141, supported by the Ministry of Education, Culture, Sports, Science and Technology (MEXT) of Japan, under The Second Earthquake and Volcano Hazards Observation and Research Program (Earthquake and Volcano Hazard Reduction Research), and supported by the short-term visiting program of the International Research Promotion Office, Earthquake Research Institute, The University of Tokyo.

Availability of data and materials

Geomagnetic field data with positioning data of the helicopter as well as the geomagnetic field data at a reference site are available from the corresponding author upon reasonable request.

Declarations**Ethics approval and consent to participate**

Not applicable.

Consent for publication

Not applicable.

Competing interests

The authors declare that they have no competing interests.

Author details

¹Earthquake Research Institute, The University of Tokyo, Yayoi 1-1-1, Bunkyo-ku, Tokyo 113-0032, Japan. ²Volcanic Fluid Research Center, Tokyo Institute of Technology, Ookayama 2-12-2, Meguro-ku, Tokyo 152-8551, Japan. ³Aso Volcanological Laboratory, Institute for Geothermal Sciences, Kyoto University, Kawayou 5280-1, Minami-Aso, Aso, Kumamoto 869-1404, Japan. ⁴Institute of Geophysics, ETH Zürich, Sonneggstrasse 5, 8092 Zürich, Switzerland. ⁵Center for Environmental Remote Sensing, Chiba University, 1-33, Yayoi-cho, Inage-ku, Chiba 268-8522 Chiba-city, Japan.

Received: 31 December 2020 Accepted: 21 June 2021

Published online: 06 July 2021

References

- Akaike H (1980) Likelihood and the Bayes procedure. *Trabajos De Estadística Y De Investigación Operativa* 31:143–166. <https://doi.org/10.1007/BF02888350>
- Akimoto T, Furuta T, Kawachi S (2002) Paleomagnetic properties of the Yatsugatake volcanic chain, Central Japan. *Bull Volcanol Soc Jpn Ser 2*(47):435–448. https://doi.org/10.18940/kazan.47.5_435 (in Japanese with English abstract)
- Bhattacharyya BK (1964) Magnetic anomalies due to prism-shaped bodies with arbitrary polarization. *Geophysics* 29:517–531. <https://doi.org/10.1190/1.1439386>
- Finlay CC, Kloss C, Olsen N, Hammer M, Toffner-Clausen L, Grayver A, Kuvshinov A (2020) The CHAOS-7 geomagnetic field model and observed changes in the South Atlantic Anomaly. *Earth Planets Space* 72:156. <https://doi.org/10.1186/s40623-020-01252-9>
- Finn AC, Sisson T, Deszcz-Pan M (2001) Aerogeophysical measurements of collapse-prone hydrothermally altered zones at Mount Rainier volcano. *Nature* 409:600–603. <https://doi.org/10.1038/35054533>
- Garmin (2007) GARMIN eTrex H personal navigator owner's manual, 1–26. https://static.garmincdn.com/pumac/eTrexH_OwnersManual.pdf. Accessed 3 June 2021
- Geometrics (2001) G-858 Magmapper operation manual, 1–106. https://geometrics.com/wp-content/uploads/2018/10/858Manual_D2.pdf. Accessed 3 June 2021
- Hansen PC (1992) Analysis of discrete ill-posed problems by means of the L-curve. *SIAM Rev* 34(4):561–580. <https://doi.org/10.1137/1034115>
- Hashimoto T, Koyama T, Kaneko T, Ohminato T, Yanagisawa T, Yoshimoto M, Suzuki E (2014) Aeromagnetic survey using an unmanned autonomous helicopter over Tarumae volcano, northern Japan. *Explor Geophys* 45:37–42. <https://doi.org/10.1071/EG12087>
- Hashimoto T, Utsugi M, Ohkura T, Kanda W, Terada A, Miura S, Iguchi M (2019) On the source characteristics of demagnetization and ground deformation associated with non-magmatic activity. *Bull Volcanol Soc Japan* 64(2):103–119. https://doi.org/10.18940/kazan.64.2_103 (in Japanese with English abstract)
- Hayakawa Y, Yui M (1989) Eruptive history of the Kusatsu Shirane volcano. *Quat Res* 28(1):1–17. <https://doi.org/10.4116/jaqua.28.1> (in Japanese with English abstract)
- Himematsu Y, Ozawa T, Aoki Y (2020) Coeruptive and posteruptive crustal deformation associated with the 2018 Kusatsu-Shirane phreatic eruption based on PALSAR-2 time series analysis. *Earth Planets Space* 72:116. <https://doi.org/10.1186/s40623-020-01247-6>
- Honsho C, Ura T, Tamaki K (2012) The inversion of deep-sea magnetic anomalies using Akaike's Bayesian information criterion. *J Geophys Res* 117:B01105. <https://doi.org/10.1029/2011JB008611>
- Kaneko T, Shimizu S, Itaya T (1991) K-Ar ages of the quaternary volcanoes in the Shin-etsu highland area, central Japan, and their formation history. *Bull Earthq Res Inst Univ Tokyo* 66:299–332 (in Japanese with English abstract)
- Kaneko T, Koyama T, Yasuda A, Takeo M, Yanagisawa T, Kajiwara K, Honda Y (2011) Low-altitude remote sensing of volcanoes using an unmanned autonomous helicopter: an example of aeromagnetic observation at Izu-Oshima volcano. *Jpn Int J Remote Sens* 32(5):1491–1504. <https://doi.org/10.1080/01431160903559770>
- Kido T, Ohnishi S, Hirajo D, Kinoshita K, Hayashi T (2016) FAZER R: industrial-use unmanned helicopter with large 32L agricultural chemical payload. *Yamaha Motor Technical Review*, Yamaha Co. Ltd. 52:78–82. https://global.yamaha-motor.com/jp/design_technology/technical/product/pdf/browse/52ss10.pdf. Accessed 3 June 2021 (in Japanese with English abstract)
- Kikawada Y, Kawai S, Shimada K, Oi T (2008) Arsenic originating in Kusatsu hot springs, Gunma, Japan, and arsenic pollution status of Kusatsu rivers. *J Disaster Res* 3(4):261–269. <https://doi.org/10.20965/jdr.2008.p0261>
- Koyama T, Kaneko T, Ohminato T, Yanagisawa T, Watanabe A, Takeo M (2013) An aeromagnetic survey of Shinmoe-dake volcano, Kirishima, Japan, after the 2011 eruption using an unmanned autonomous helicopter. *Earth Planets Space* 65:657–666. <https://doi.org/10.5047/eps.2013.03.005>
- Koyama T, Kaneko T, Ohminato T, Watanabe A, Honda Y (2019) Aeromagnetic survey by drone in Iwoyama, Kirishima volcano. In: Abstract of SGEPPS fall meeting 2019, Kumamoto, 23–27 Oct 2019. <http://www.sgepps.org/sgepps/sookai/146/html/program/pdf/R003/R003-P04.pdf>. Accessed 3 June 2021 (in Japanese with English abstract)
- Kunaratnam K (1981) Simplified expressions for the magnetic anomalies due to vertical rectangular prisms. *Geophys Prospect* 29:883–890. <https://doi.org/10.1111/j.1365-2478.1981.tb01032.x>
- Li Y, Oldenburg DW (1996) 3-D inversion of magnetic data. *Geophysics* 61(2):394–408. <https://doi.org/10.1190/1.1443968>
- Li Y, Oldenburg DW (2000) Joint inversion of surface and three-component borehole magnetic data. *Geophysics* 65(2):540–552. <https://doi.org/10.1190/1.1444749>
- Malehmir A, Dynesius L, Paulusson K, Johansson R, Bastani M, Wedmark M, Marsden P (2017) The potential of rotary-wing UAV-based magnetic surveys for mineral exploration: a case study from central Sweden. *Lead Edge* 36(7):552–557. <https://doi.org/10.1190/le36070552.1>
- Matsunaga Y, Kanda W, Takakura S, Koyama T, Saito Z, Seki K, Suzuki A, Kishita T, Kinoshita Y, Ogawa Y (2020) Magmatic hydrothermal system inferred from the resistivity structure of Kusatsu-Shirane volcano. *J Volcanol Geotherm Res* 390:106742. <https://doi.org/10.1016/j.jvolgeores.2019.106742>
- Morimoto T (2017) Introduction to the satellite-based long-distance, programmable-navigation operation of the FAZER R G2. *Yamaha Motor Technical Review*, Yamaha Co. Ltd. 53:9–13. https://global.yamaha-motor.com/jp/design_technology/technical/presentation/pdf/browse/53gs02.pdf. Accessed 3 June 2021 (in Japanese with English abstract)
- Nagai M, Ueki K, Mizuno Y, Tanaka Y, Inui M, Nogami K, Tanada T (2015) Stratigraphy and radiometric ages of volcanic rocks from the drill hole of the Hoshimata observation station of Kusatsu-Shiranesan volcano, Central Japan. In: Abstract of Volcanological Society of Japan 2015 fall meeting, Toyama, 27 Sep–2 Oct 2015. https://www.jstage.jst.go.jp/article/vsj/2015/0/2015_113/_pdf/-char/ja. Accessed 3 June 2021 (in Japanese)
- Nakatsuka T (1994) Aeromagnetic anomalies over the area of Unzendake volcano. *J Geomag Geoelectr* 46:529–540. <https://doi.org/10.5636/jgg.46.529>
- Nakatsuka T, Okuma S (2014) Aeromagnetic 3D subsurface imaging with effective source volume minimization and its application to data from the Otoge cauldron, Shitara, Central Japan. *Explor Geophys* 45:16–23. <https://doi.org/10.1071/EG13022>

- Nigorikawa A, Ishizaki Y, Kametani N, Yoshimoto M, Terada A, Ueki K, Nakamura K (2016) Holocene eruptive history of the Motoshirane Pyroclastic Cone Group, Kusatsu-Shirane volcano. In: Abstract of Japan geoscience union meeting 2016, Makuhari, Chiba, 22–26 May 2016. <https://confit.atlas.jp/guide/event/jpgu2016/subject/SVC48-11/detail>. Accessed 3 June 2021
- Ogawa Y, Aoyama H, Yamamoto M, Tsutsui T, Terada A, Ohkura T, Kanda W, Koyama T, Kaneko T, Ohminato T, Ishizaki Y, Yoshimoto M, Ishimine Y, Nogami K, Mori T, Kikawada Y, Kataoka K, Matsumoto T, Kamiisi I, Yamaguchi S, Ito Y, Tsunematsu K (2018) Comprehensive survey of 2018 Kusatsu-Shirane Eruption. In: Proc. Symp. on the natural disaster sciences, 55:25–30 (in Japanese)
- Ohba T, Hirabayashi J, Nogami K (2000) D/H and $^{18}\text{O}/^{16}\text{O}$ ratios in the crater lake at Kusatsu-Shirane volcano, Japan. *J Volcanol Geotherm Res* 97:329–346. [https://doi.org/10.1016/S0377-0273\(99\)00169-9](https://doi.org/10.1016/S0377-0273(99)00169-9)
- Ohminato T, Kaneko T, Koyama T, Watanabe A, Kanda W, Tameguri T, Kazahaya R (2017) Observations using an unmanned aerial vehicle in an area in danger of volcanic eruptions at Kuchinoerabu-jima volcano, southern Kyushu. *Jpn J Nat Disaster Sci* 38(1):85–104. <https://doi.org/10.2328/jnds.38.85>
- Okubo A, Tanaka Y, Utsugi M, Kitada N, Shimizu H, Matsushima T (2005) Magnetization intensity mapping on Unzen volcano, Japan, determined from high-resolution, low-altitude helicopter-borne aeromagnetic survey. *Earth Planets Space* 57:743–753. <https://doi.org/10.1186/BF03351853>
- Okuma S, Makino M, Nakatsuka T (1994) Magnetization intensity mapping in and around Izu-Oshima volcano, Japan. *J Geomag Geoelectr* 46:541–556. <https://doi.org/10.5636/jgg.46.541>
- Takahashi K, Fujii I (2014) Long-term thermal activity revealed by magnetic measurements at Kusatsu-Shirane volcano, Japan. *J Volcanol Geotherm Res* 285:180–194. <https://doi.org/10.1016/j.jvolgeores.2014.08.014>
- Terada A (2018) Kusatsu-Shirane volcano as a site of phreatic eruptions. *Jour Geol Soc Japan* 124(4):251–270. <https://doi.org/10.5575/geosoc.2017.0060> (in Japanese with English abstract)
- Tseng KH, Ogawa Y, Nurhasan TSB, Ujihara N, Honkura Y, Terada A, Usui Y, Kanda W (2020) Anatomy of active volcanic edifice at the Kusatsu-Shirane volcano, Japan, by magnetotellurics: hydrothermal implications for volcanic unrests. *Earth Planets Space* 72:161. <https://doi.org/10.1186/s40623-020-01283-2>
- Uto K, Kurihara A, Hirabayashi J (2004) Core descriptions of seismological observation wells around Shirane cone, Kusatsu Shirane volcano. Report of 4th joint observation of Kusatsu-Shirane volcano 59–68. <http://www.ksv.titech.ac.jp/jpn/kusatsu-2003-shuchu-report/08-Uto.pdf>. Accessed 3 June 2021 (in Japanese)
- Utsugi M (2019) 3-D inversion of magnetic data based on the L1–L2 norm regularization. *Earth Planets Space* 71:73. <https://doi.org/10.1186/s40623-019-1052-4>
- Utsugi M, Hashimoto T (2016) Development of the aeromagnetic survey system using drone multicopter. In: Abstract of SGEPS fall meeting 2016, Fukuoka, 19–23 Nov 2016. <http://www.sgeps.org/sgeps/sookai/140/html/program/pdf/R003/R003-P11.pdf>. Accessed 3 June 2021
- Wessel P, Smith WHF, Scharroo R, Luis J, Wobbe F (2013) Generic mapping tools: improved version released. *EOS Trans AGU* 94(45):409–410. <https://doi.org/10.1002/2013EO45001>
- Yamazaki A, Churei M, Tsunomura S, Nakajima S (1992) Analysis of the variation of geomagnetic total force at the Kusatsu-Shirane volcano: the remarkable changes in the geomagnetic total force in 1990 and the estimated thermal demagnetization model. *Memoirs of the Kakioka Magnetic Observatory* 24(2):53–66. https://www.kakioka-jma.go.jp/publ/journal_DB/pdf_files/technical_report_of_KMO_sup_03_02.pdf. Accessed 3 June 2021 (English translation, original in Japanese)

Publisher's Note

Springer Nature remains neutral with regard to jurisdictional claims in published maps and institutional affiliations.

Submit your manuscript to a SpringerOpen[®] journal and benefit from:

- Convenient online submission
- Rigorous peer review
- Open access: articles freely available online
- High visibility within the field
- Retaining the copyright to your article

Submit your next manuscript at ► [springeropen.com](https://www.springeropen.com)
